

On the range of validity of perturbative models for galaxy clustering and its uncertainty

Giosuè Gambardella,^{1,2} Matteo Biagetti,^{3,2,4} Chiara Moretti,^{4,7,2,5} and Emiliano Sefusatti^{5,2,6}

¹*Dipartimento di fisica, Università di Trieste, via Valerio 2, 34127 Trieste, Italy*

²*Institute for Fundamental Physics of the Universe, Via Beirut 2, 34151 Trieste, Italy*

³*Area Science Park, Località Padriciano 99, 34149 Trieste, Italy*

⁴*Scuola Internazionale di Studi Superiori Avanzati, via Bonomea 265, 34136 Trieste, Italy*

⁵*Istituto Nazionale di Astrofisica, Osservatorio Astronomico di Trieste, via Tiepolo 11, 34143 Trieste, Italy*

⁶*Istituto Nazionale di Fisica Nucleare, Sezione di Trieste, via Valerio 2, 34127 Trieste, Italy and*

⁷*Centro Nazionale "High Performance Computer, Big Data and Quantum Computing"*

(Dated: November 9, 2023)

We explore the reach of analytical models at one-loop in Perturbation Theory (PT) to accurately describe measurements of the galaxy power spectrum from numerical simulations in redshift space. We consider the validity range in terms of three different diagnostics: 1) the goodness of fit; 2) a figure-of-bias quantifying the error in recovering the fiducial value of a cosmological parameter; 3) an internal consistency check of the theoretical model quantifying the running of the model parameters with the scale cut. We consider different sets of measurements corresponding to an increasing cumulative simulation volume in redshift space. For each volume we define a median value and the associated scatter for the largest wavenumber where the model is valid (the k -reach of the model). We find, as a rather general result, that the median value of the reach decreases with the simulation volume, as expected since the smaller statistical errors provide a more stringent test for the model. This is true for all the three definitions considered, with the one given in terms of the figure-of-bias providing the most stringent scale cut. More interestingly, we find as well that the error associated with the k -reach value is quite large, with a significant probability of being as low as $0.1 h \text{ Mpc}^{-1}$ (or, more generally, up to 40% smaller than the median) for all the simulation volumes considered. We explore as well the additional information on the growth rate parameter encoded in the power spectrum hexadecapole, compared to the analysis of monopole and quadrupole, as a function of simulation volume. While our analysis is, in many ways, rather simplified, we find that the gain in the determination of the growth rate is quite small in absolute value and well within the statistical error on the corresponding figure of merit.

I. INTRODUCTION

The theoretical modelling of the galaxy power spectrum in redshift space has witnessed, over the past two decades, significant advancements in terms of an accurate description, at the one-loop level, of nonlinear matter evolution, galaxy bias, and redshift-space distortions (see, e.g. [1–4] for some recent analyses). The range of scales included in the analysis of a given power spectrum measurement can be limited by the reach of the theoretical model, determined by the perturbative order of the model and, ultimately, by distinct characteristic scales determined by the nonlinear matter evolution, non-local galaxy bias, redshift-space distortions as well as possible corrections to Poisson shot-noise.

Despite some valuable efforts [5, 6], the various and complex physical processes at play do not allow a simple but accurate estimate of theoretical error due to neglecting higher-order corrections. For this reason, in practice, the range of validity of the model is determined in actual data analysis by comparing results varying the maximum wavenumber k_{max} making sure the posteriors on cosmological parameters are not running. In [7, 8] the effect on parameters constraints of representative next-order corrections is also considered in the determination of k_{max} . This, of course, still depends, inevitably, on the specific realisation of the galaxy and matter distributions. Alternatively, the "scale cut" could be determined by comparison to N-body simulations (see [3, 9]). The scale-cut will then be applied to a data set again affected by statistical scatter. The question is then how conservative should this choice be to account for such scatter. All these approaches are affected, in

different ways, by statistical errors, in addition to other limitations, as, for instance, the reliability of N-body simulations and the synthetic galaxy catalog.

In this paper, we provide a simple numerical exploration of this issue. Specifically, we study of how the range of validity of a one-loop PT model for the galaxy power spectrum multipoles in redshift space, determined from a single measurement over a given volume, is affected by the statistical error. We do so considering a very large set of simulated galaxy catalogs, the SANCHO data set, and considering the mean of power spectrum measurements from subsets of increasing size, therefore corresponding to an increasing effective volume. For each value of the subset cumulative volume, we derive scale cut estimates from all available subsets, and therefore an estimate of its scatter. We proceed to study these results as a function of the cumulative volume.

This paper is organised as follows. In section II we present the simulations data set, the power spectrum measurements, and their covariance. In section III we present the methodology, with a brief mention of the theoretical model and parameters implemented in the inference pipeline, and a description of the Likelihood analysis. In section IV we present our results and conclusions.

II. DATA AND MEASUREMENTS

The SANCHO dataset. In this work we make use of galaxy mock catalogs from the SANCHO suite[10]. The complete SANCHO data-set encompasses 240,000 galaxy

mocks in redshift space scanning across 11 cosmologies, 3 massive neutrino cosmologies, 6 primordial non-Gaussianity amplitudes, and 11 Halo Occupation Distribution (HOD) models. These catalogs are based on the QUIJOTE N-body simulations [11], run with 512^3 dark matter particles in a box of volume $1 h^{-3} \text{Gpc}^3$. Galaxies are populated on halo catalogs using a 5 parameter Halo Occupation Distribution (HOD) model, as described in [12]. The HOD parameters are chosen such that the catalogs mock the CMASS galaxies observed by BOSS [13], the average number density being $\bar{n}_g \approx 3 \times 10^{-4} h^3 \text{Gpc}^{-3}$ at redshift $z = 0.5$. In this work, we use a subset of almost 5,000 catalogs from the fiducial cosmology set, a ΛCDM cosmology with $\Omega_m = 0.3175$, $\Omega_b = 0.049$, $h = 0.6711$, $n_s = 0.9624$, $\sigma_8 = 0.834$ and $\sum m_\nu = 0.0 \text{eV}$.

Measurements and covariance The galaxy power spectrum monopole, quadrupole, and hexadecapole in redshift space ($P_\ell(k)$ with $\ell = \{0, 2, 4\}$) are measured using the public code PBI4[14] [15]. The code computes the density grid using a fourth-order mass-assignment scheme with interlacing as described in [16]. The wavenumbers bins have a width of $\Delta k = 2k_f$, where $k_f = 0.006 h \text{Mpc}^{-1}$ is the fundamental frequency of the SANCHO box, and are computed up to $k_{\text{max}} = 0.45 h \text{Mpc}^{-1}$. These measurements are publicly available along with the SANCHO dataset. The covariance used in the analysis is estimated numerically from these measurements as

$$\hat{C}_{ij}^{\ell\ell'} = \langle [\hat{P}_\ell^{(\alpha)}(k_i) - \langle \hat{P}_\ell^{(\alpha)}(k_i) \rangle] [\hat{P}_{\ell'}^{(\alpha)}(k_j) - \langle \hat{P}_{\ell'}^{(\alpha)}(k_j) \rangle] \rangle \quad (1)$$

where $\hat{P}_\ell^{(\alpha)}(k)$ is the α -th measurement of the power spectrum multipoles, while the expectation value $\langle \dots \rangle$ is obtained as the average over the fiducial cosmology simulations set comprising 4,000 realisations. Given this large number and a data vector size not larger (but in most cases much smaller) than 108, we ignore statistical errors affecting the resulting covariance (see, e.g.[17]).

III. METHODOLOGY

A. Theoretical model

We consider the next-to-leading order prescription for the galaxy power spectrum multipoles in redshift space implemented in the PBJ code adopted in [18–22]. We refer the reader to these works for a proper description of the theoretical prediction. This corresponds to the Effective Field Theory of Large-Scale Structure model tested in the challenge paper of [23] and employed, for instance, in the analyses of the BOSS data in [2, 3]. In brief, we adopt the following bias expansion up to the third order,

$$\delta_g = b_1 \delta + \frac{b_2}{2} \delta^2 + b_{\mathcal{G}_2} \mathcal{G}_2 + b_{\Gamma_3} \Gamma_3 + \epsilon \quad (2)$$

where b_1 and b_2 are respectively the linear and quadratic bias while \mathcal{G}_2 and Γ_3 are two Galileon operators which quantify

non local effects on the density field. The expression for the galaxy power spectrum in redshift-space is given by

$$\begin{aligned} P_g(\mathbf{k}) &= Z_1^2(\mathbf{k}) P_L(k) \\ &+ 2 \int d^3 \mathbf{q} [Z_2(\mathbf{q}, \mathbf{k} - \mathbf{q})]^2 P_L(q) P_L(|\mathbf{k} - \mathbf{q}|) \\ &+ 6 Z_1(\mathbf{k}) P_L(k) \int d^3 \mathbf{q} Z_3(\mathbf{k}, \mathbf{q}, -\mathbf{q}) P_L(q) \\ &+ P_{\text{noise}}(\mathbf{k}) + P_{\text{ctr}}(\mathbf{k}). \end{aligned} \quad (3)$$

where $Z_1(\mathbf{k})$, $Z_2(\mathbf{k}_1, \mathbf{k}_2)$ and $Z_3(\mathbf{k}_1, \mathbf{k}_2, \mathbf{k}_3)$ are the usual redshift-space kernels (see, for instance, [2] for their full expression corresponding to the adopted bias expansion). The last two terms in the eq. (3) are the contributions from shot-noise and the EFT counterterms. The first is given by

$$P_{\text{noise}}(k, \mu) = \frac{1}{\bar{n}} \left[(1 + \alpha_P + \epsilon_{0,k^2} k^2 + \epsilon_{2,k^2} k^2 \mu^2) \right] \quad (4)$$

where \bar{n} is the (known) mean number density of objects while the parameters α_P , ϵ_{0,k^2} and ϵ_{2,k^2} describe constant and scale-dependent deviations from the Poisson prediction. In the expression above and in what follows, μ represents the cosine of the angle formed by the line of sight and the wavevector \mathbf{k} . The EFT counterterms contribution is given instead by

$$\begin{aligned} P_{\text{ctr}}(k, \mu) &= -2\tilde{c}_0 k^2 P_L(k) - 2\tilde{c}_2 k^2 f \mu^2 P_L(k) \\ &- 2\tilde{c}_4 k^2 f^2 \mu^4 P_L(k) \\ &+ c_{\nabla^4 \delta} (\mu k f)^4 (b_1 + f \mu^2)^2 P_L(k). \end{aligned} \quad (5)$$

The power spectrum multipoles are then defined as

$$P_\ell(k) \equiv \frac{(2\ell + 1)}{2} \int d\mu P_g(\mathbf{k}) P_\ell(\mu), \quad (6)$$

where $P_\ell(\mu)$ are the l-order Legendre polynomials.

In order to accurately describe the nonlinear evolution of the acoustic features we implement the Infrared Resummation [24] following [25] with the wiggle-no wiggle split from the 1D Gaussian filter method described in [26].

The model depends on 7 bias and shot-noise parameters plus 4 counterterms, in addition to the cosmological parameters. These are reduced to 6 and 3 when only monopole and quadrupole are considered. Given the large number of fits we perform, we fix all cosmological parameters to their fiducial value: this allows us to avoid re-computing the linear power spectrum and the PT contributions at each step in the Markov chain, leading to a significant speed up in the analysis. However, we keep as a free parameter the growth rate parameter f , to be used as a proxy for the cosmological parameters in the definition of the figure of bias.

Since we explore only parameters that can be factorised in each contribution to the full power spectrum multipoles, we can also account exactly for the effect of wavenumber bins adopted by the estimator. We do so by considering the average of the model over the discrete wavenumbers falling into each k -bin, following the procedure described in section 3.2 of [19].

Parameter	Prior
b_1	$\mathcal{U}(0.9, 3.5)$
b_2	$\mathcal{U}(-4, 4)$
$b_{\mathcal{G}_2}$	$\mathcal{U}(-4, 4)$
b_{Γ_3}	$\mathcal{U}(-10, 10)$
α_P	$\mathcal{U}(-1, 1)$
ϵ_{k^2}	$\mathcal{U}(-10, 10)$
ϵ_{k^4}	$\mathcal{U}(-100, 100)$
c_0	$\mathcal{U}(-100, 100)$
c_2	$\mathcal{U}(-500, 500)$
c_4	$\mathcal{U}(-500, 500)$
$c_{\nabla^4 \delta}$	$\mathcal{U}(-500, 500)$
f	$\mathcal{U}(0.1, 1)$

TABLE I. Uniform priors for the model parameters adopted in the analysis.

B. Likelihood analysis

We assume a Gaussian likelihood for the data vector corresponding to the three power spectrum multipoles $\{P_0(k_1), \dots, P_2(k_1), \dots, P_4(k_1), \dots\}$ where each observable is limited in range by a chosen k_{\max} .

For each measurement α we define the log-likelihood

$$\begin{aligned} \ln \mathcal{L}_\alpha &\equiv -\frac{1}{2} \chi_\alpha^2 \\ &\equiv -\frac{1}{2} \sum_{\ell, \ell'} \sum_{k_i, k_j}^{k_{\max}} \delta P_\ell^{(\alpha)}(k_i) [\hat{C}^{-1}]_{ij}^{\ell \ell'} \delta P_{\ell'}^{(\alpha)}(k_j), \end{aligned} \quad (7)$$

where $\delta P_\ell^{(\alpha)}(k_i) \equiv \hat{P}_\ell^{(\alpha)}(k_i) - P_\ell^{\text{th}}(k_i)$ and $[\hat{C}^{-1}]_{ij}^{\ell \ell'}$ denotes a generic element of the inverse of the full covariance matrix for the data vector obtained by joining the three multipoles.

The log-likelihood corresponding to a set of N_R data vector measurements is given by the sum

$$\ln \mathcal{L}_{\text{tot}} = \sum_{\alpha=1}^{N_R} \ln \mathcal{L}_\alpha = -\frac{1}{2} \sum_{\alpha=1}^{N_R} \chi_\alpha^2. \quad (8)$$

We adopt uniform priors for all parameters, as detailed in table I.

The evaluation of the posterior distribution has been performed by running Monte Carlo Markov Chain (MCMC) simulations with the affine invariant sampler implemented in the emcee package [27]. We choose to run the MCMC with 50 walkers and 50000 steps. We ensure the convergence stopping the chains after 50 autocorrelation times.

C. Diagnostics

To determine the range of validity of the model, parametrized by the maximum wavenumber k_{\max} , we con-

sider three different diagnostics: the goodness of fit (GoF), a figure-of-bias (FoB) quantifying systematic errors in the recovery of the fiducial value for a cosmological parameter and an additional consistency test. We describe them below.

Goodness of fit For the evaluation of the goodness of fit we compute the reduced chi-square statistic $\chi_{\text{red}}^2 = \chi_{\text{tot}}^2 / N_{\text{dof}}$, N_{dof} being the number of degrees of freedom. The χ_{tot}^2 is computed as an average over the posterior. If, for a given value of k_{\max} , the reduced chi-square falls outside the 95% confidence interval expected for the value of N_{dof} , the model “fails” and we set the reach of the model equal to the previous k_{\max} value.

Figure of bias (FoB) With the figure of bias we estimate the size of the systematic error induced by the model on the cosmological parameters, as a function of k_{\max} . As mentioned already, in this work we limit our attention to the growth rate parameter f , since the analysis of the full set of cosmological parameters, to the extent of the one conducted here, would be computationally too demanding. We define the figure of bias for the parameter f as

$$\text{FoB} = \frac{|\hat{f}(k_{\max}) - f_{\text{fid}}|}{\sigma_f(k_{\max})}, \quad (9)$$

where f_{fid} is the value of f corresponding to the fiducial cosmology while σ_f is the marginalised error on f at that k_{\max} value. The reach of the model based on the FoB, $k_{\text{reach}}^{\text{FoB}}$, is then defined by the largest value of k_{\max} such that $\text{FoB} < 2$.

Consistency Finally we consider a “consistency” criterion based on the fact that all model parameters are constant and therefore not expected to depend on the scale k_{\max} , since this would indicate a clear failure of the model. We identify a possible running of a parameter by performing a fit of all its values at different k_{\max} with a constant function. We then compute the reduced chi-square of the fit and compare it with the 95% confidence interval, determining for each parameter the reach of the model in the same way as in the goodness of fit. The reach of the model based on the consistency criterion will then be the minimum k_{reach} across the different parameters.

It is clear that the definition of the range of acceptable values for each of these statistics is somewhat arbitrary. We made the choice of having our three definitions correspond to a 95% probability interval, in order to have, to some extent, more homogeneous results. A looser definition (i.e. a larger confidence interval) on the model reach, for all diagnostics, lead to qualitatively similar results with higher values for the median k_{reach} , as expected, but comparable scatter.

N_{sub}	6	13	16	24	48	72	88	200	306	400	580	1160
V_{tot}	666	307	250	166	83	55	45	20	13	10	6	3

TABLE II. Simulations subsets. Here N_{sub} is the number of realisations subsets for a given cumulative simulation volume V_{tot} (in $h^{-3} \text{Gpc}^3$). The value $V_{\text{tot}}/(h^{-3} \text{Gpc}^3)$ corresponds as well to the number of simulations in each subset, N_{sim} , since each individual simulation has a volume of $1 h^{-3} \text{Gpc}^3$.

IV. RESULTS AND CONCLUSIONS

A. Model reach and its uncertainty

We investigate the reach of the model as a function of the size of statistical errors affecting the power spectrum measurements. We do so by considering increasingly large subsets of distinct measurements corresponding to twelve values for the cumulative simulation volume from 3 to $600 h^{-3} \text{Gpc}^3$, as detailed in table II. From each set characterized by a given cumulative volume we extract three values of k_{reach} according to the different definitions, while we obtain an estimate of its error from the scatter across all subsets of the same size. We consider k_{max} values in the range $k_{\text{max}} \in \{0.04, 0.44\} h \text{Mpc}^{-1}$ separated by the interval $\Delta k_{\text{max}} = 0.04 h \text{Mpc}^{-1}$.

In the top panel of figure 1 we show the median of the reach of the model for the joint analysis of monopole, quadrupole and hexadecapole as a function of the cumulative simulation volume V . The blue, red and green points denote the k_{reach} defined, respectively, from the goodness of fit, the figure of bias and from the model consistency test. The shaded area fills the interval between the 16th and 84th percentile in the distribution of values across the distinct subsets of equal volume. The bottom panel shows the relative scatter with respect to the median. The first two vertical gray lines from the left mark, approximately, the volume of a typical redshift bin of the BOSS CMASS sample ($3 h^{-3} \text{Gpc}^3$, [29]) and of the Euclid spectroscopic sample ($10 h^{-3} \text{Gpc}^3$ [30]) while the third one on the right corresponds to the total simulation volume of $566 h^{-3} \text{Gpc}^3$ adopted in the PT challenge paper of [28].

As expected, the k_{reach} decreases as the volume increases, that is with decreasing statistical errors. We notice that the scatter as well becomes smaller for larger volumes, for all the definitions of k_{reach} , although for the largest volumes this estimate is also affected by the smaller number of subsets. The different definitions appear to be largely consistent with each other, with the FoB providing the most stringent definition of k_{reach} , and the smallest scatter. The GoF and the consistency criterion are instead characterised by larger median k_{reach} , with the latter also showing a larger variability in the scatter as a function of volume.

Perhaps the most interesting result is the quite significant size of the scatter affecting all k_{reach} estimates. For nearly all volumes considered the model reach can be below $0.1 h \text{Mpc}^{-1}$ with considerable probability, while the upper limit is of the order of 20-25% larger than the median value. We notice that

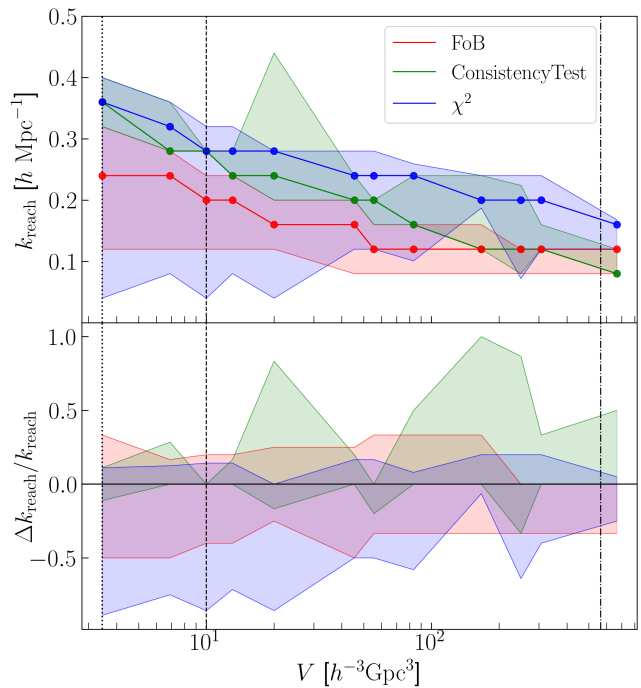


FIG. 1. In the top panel we show the median of the k_{reach} with the inclusion of the hexadecapole in the analysis, estimated with the three different methods, as a function of the cumulative volume V . The shaded areas represent the 16th percentile and the 84th percentile. In the bottom panel we show the relative scatter with respect to the median, for the three methods. The three vertical lines represent the volume of a typical redshift bin for BOSS (dotted line), a Euclid-like survey (dashed line) and the total volume adopted in the modelling challenge of [28] (dash-dotted line).

for the smallest volumes considered this last result could be affected by the largest value of $k_{\text{max}} = 0.44 h \text{Mpc}^{-1}$ considered for the measurements, but should be robust for most cases.

It is also interesting to notice that the theory consistency test is failed first by the $c_{\nabla^4 \delta}$ counterterm, describing higher order Finger-of-God effects[31]. This happens, notably, for the small volumes that are closer to those relevant for realistic surveys, for which the model is valid up to larger k values. At larger volumes, where the range is more limited and nonlinear corrections are less relevant and perhaps properly described in terms of one-loop corrections, the parameter to fail first is the linear bias b_1 , maybe because other, nonlinear, parameters are relatively less constrained.

B. Hexadecapole information

The overall picture described in the previous section does not change significantly when the hexadecapole is excluded from the analysis. The median k_{reach} is also not noticeably different, and not consistently larger either, indicating the relatively small constraining power this observable has on the model.

The results above, however, allow to investigate any additional information provided by the hexadecapole, at least on the growth rate f , and how this is affected by statistical errors. To this end, we define a Figure of Merit (FoM) on such parameter given simply by the inverse of its marginalised uncertainty

$$\text{FoM} = \frac{1}{\sigma_f(k_{\max})}. \quad (10)$$

We consider MCMC runs with the conservative choice $k_{\max} = k_{\text{reach}}^{\text{FoB}}$ and extract the uncertainty on the parameter f from its posterior distribution. As a final result, we can obtain the figure of merit as a function of the cumulative volume.

The top panel of figure 2 shows the median value of the figure of merit across all simulation subsets of equal volume along with its scatter for both analyses, including and excluding the hexadecapole information. We see how, as we can expect, the FoM grows as the volume increases, although such increase tends to flatten at the highest volumes. This is likely due to the reduced range of the analysis for these configurations. The scatter also grows significantly with the volume. Remarkably, the difference induced by the addition of the hexadecapole is quite small, and significantly smaller than the scatter. This also makes not too relevant the relatively larger FoM for the $P_0 - P_2$ -only analysis for some cases at large cumulative volume.

This is more clearly shown in the bottom panel of figure 2, where we plot the median relative difference due to P_4 evaluated for each subset. The improvement is consistent with zero for all volumes considered, with a very wide large scatter associated to this quantity.

These results suggest that the hexadecapole does not provide, *on average*, additional information on the growth rate parameter. It is still true that, in a small but sizeable fraction of realisations close to the characteristic volume of current redshift surveys, the improvement on the FoM could correspond to $\sim 50\%$.

C. Discussion

The determination of conservative scale-cuts in the analysis of observational data-sets is quite an important decision to be made, as it is necessary to avoid introducing systematic errors due to the limitations of the theoretical model. On the other hand, it is also crucial to take advantage of the available information as much as possible.

In principle a scale-cut can be defined from a proper estimate of the theoretical error (see, e.g. [5]) compared to a numerical or analytical estimate of the statistical uncertainty. Unfortunately, theory errors could not be determined so far with sufficient accuracy to be used in practice for this purpose.

We provided here a first simple, but extensive, assessment of the statistical errors affecting the determination of the validity range of the theory according to three criteria. In the analysis of actual data, of course, the FoB considered here cannot be used for the determination of the scale cuts, while the consistency test is the typical, practical choice. We find, however, that the k_{reach} determined with the latter is consistently higher than the one from the FoB, and it could therefore allow some

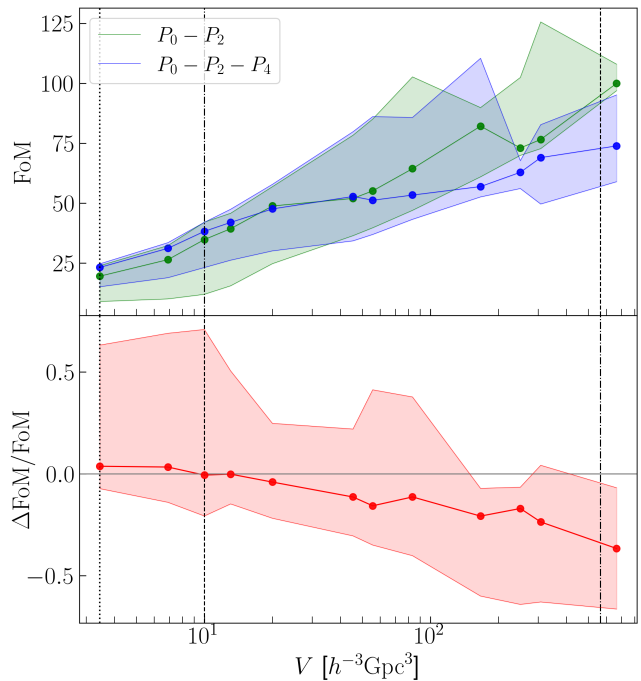


FIG. 2. The plot in the top panel shows the median of the Figure of Merit, with the inclusion of the hexadecapole (bue) and without it (green), as a function of the volume V . In the bottom panel we plot the relative median of the differences of the Figures of Merit, with the inclusion of the hexadecapole and without it, against the volume V . The shaded areas represent the 16th percentile and the 84th percentile. The three vertical lines represent respectively the volume of a typical redshift bin for BOSS (dotted), a Euclid-like survey (dashed) and the total volume adopted in the modelling challenge of [28] (dot-dashed).

level of systematic error on the determination of cosmological parameters. In addition it is also characterised by a scatter with a significant variability across the cumulative volumes considered here.

Our work is limited in many ways. It focuses on a single parameter, f , as a proxy for the whole set of cosmological parameters. It considers a single theoretical model with a given choice of priors while it would be interesting to see how a comparison between different theoretical assumptions or phenomenological models would look like when conducted on a large subsets of catalogs with variable cumulative volume.

Even our basic assessment of the amount of information in the power spectrum hexadecapole could benefit from a more general likelihood analysis perhaps considering alternative statistics to limit FoG effects [32, 33].

We leave these possible explorations to future work.

ACKNOWLEDGEMENTS

We are grateful to Pierluigi Monaco, Cristiano Porciani and Marko Simonović for helpful discussions and valuable suggestions. M.B. is supported by the Programma Nazionale della Ricerca (PNR) grant J95F21002830001 with title "FAIR-by-

design". CM's work is supported by the Fondazione ICSC, Spoke 3 Astrophysics and Cosmos Observations, National Recovery and Resilience Plan (Piano Nazionale di Ripresa e Resilienza, PNRR) Project ID CN_00000013 "Italian Research Center on High-Performance Computing, Big Data and

Quantum Computing" funded by MUR Missione 4 Componente 2 Investimento 1.4: Potenziamento strutture di ricerca e creazione di "campioni nazionali di R&S (M4C2-19)" - Next Generation EU (NGEU).

-
- [1] S. Alam, M. Ata, S. Bailey, F. Beutler, D. Bizyaev, J. A. Blazek, A. S. Bolton, J. R. Brownstein, A. Burden, C.-H. Chuang, et al., *MNRAS* **470**, 2617 (2017), 1607.03155.
- [2] M. M. Ivanov, M. Simonović, and M. Zaldarriaga, *J. Cosmology Astropart. Phys.* **2020**, 042 (2020), 1909.05277.
- [3] G. d'Amico, J. Gleyzes, N. Kokron, K. Markovic, L. Senatore, P. Zhang, F. Beutler, and H. Gil-Marín, *J. Cosmology Astropart. Phys.* **2020**, 005 (2020), 1909.05271.
- [4] A. Semenaite, A. G. Sánchez, A. Pezzotta, J. Hou, R. Scocimarro, A. Eggemeier, M. Crocche, C.-H. Chuang, A. Smith, C. Zhao, et al., *MNRAS* **512**, 5657 (2022), 2111.03156.
- [5] T. Baldauf, M. Mirbabayi, M. Simonović, and M. Zaldarriaga, *ArXiv e-prints* (2016), 1602.00674.
- [6] A. Chudaykin, M. M. Ivanov, and M. Simonović, *Phys. Rev. D* **103**, 043525 (2021), 2009.10724.
- [7] P. Zhang, G. D'Amico, L. Senatore, C. Zhao, and Y. Cai, *J. Cosmology Astropart. Phys.* **2022**, 036 (2022), 2110.07539.
- [8] G. D'Amico, Y. Donath, M. Lewandowski, L. Senatore, and P. Zhang, *arXiv e-prints arXiv:2206.08327* (2022), 2206.08327.
- [9] M. M. Ivanov, O. H. E. Philcox, G. Cabass, T. Nishimichi, M. Simonović, and M. Zaldarriaga, *Phys. Rev. D* **107**, 083515 (2023), 2302.04414.
- [10] Note1, documentation and free access to the full suite is found here.
- [11] F. Villaescusa-Navarro, C. Hahn, E. Massara, A. Banerjee, A. M. Delgado, D. K. Ramanah, T. Charnock, E. Giusarma, Y. Li, E. Allys, et al., *ApJS* **250**, 2 (2020), 1909.05273.
- [12] Z. Zheng, A. L. Coil, and I. Zehavi, *ApJ* **667**, 760 (2007), *arXiv:astro-ph/0703457*.
- [13] F. Beutler, H.-J. Seo, A. J. Ross, P. McDonald, S. Saito, A. S. Bolton, J. R. Brownstein, C.-H. Chuang, A. J. Cuesta, D. J. Eisenstein, et al., *MNRAS* **464**, 3409 (2017), 1607.03149.
- [14] Note2, <https://github.com/matteobiagetti/pbi4>.
- [15] M. Biagetti, F. Verdiani, and E. Sefusatti, *Pbi4* (2023), URL <https://zenodo.org/records/10008045>.
- [16] E. Sefusatti, M. Crocche, R. Scocimarro, and H. M. P. Couchman, *MNRAS* **460**, 3624 (2016), 1512.07295.
- [17] W. J. Percival, A. J. Ross, A. G. Sánchez, L. Samushia, A. Burden, R. Crittenden, A. J. Cuesta, M. V. Magana, M. Manera, F. Beutler, et al., *MNRAS* **439**, 2531 (2014), 1312.4841.
- [18] A. Oddo, E. Sefusatti, C. Porciani, P. Monaco, and A. G. Sánchez, *J. Cosmology Astropart. Phys.* **2020**, 056 (2020), 1908.01774.
- [19] A. Oddo, F. Rizzo, E. Sefusatti, C. Porciani, and P. Monaco, *J. Cosmology Astropart. Phys.* **2021**, 038 (2021), 2108.03204.
- [20] P. Carrilho, C. Moretti, B. Bose, K. Markovič, and A. Poursidou, *J. Cosmology Astropart. Phys.* **2021**, 004 (2021), 2106.13163.
- [21] P. Carrilho, C. Moretti, and A. Poursidou, *J. Cosmology Astropart. Phys.* **2023**, 028 (2023), 2207.14784.
- [22] C. Moretti, M. Tsedrik, P. Carrilho, and A. Poursidou, *arXiv e-prints arXiv:2306.09275* (2023), 2306.09275.
- [23] T. Nishimichi, *J. Cosmology Astropart. Phys.* **2012**, 037 (2012), 1204.3490.
- [24] L. Senatore and M. Zaldarriaga, *ArXiv e-prints* (2014), 1409.1225.
- [25] T. Baldauf, M. Mirbabayi, M. Simonović, and M. Zaldarriaga, *Phys. Rev. D* **92**, 043514 (2015), 1504.04366.
- [26] Z. Vlah, U. Seljak, M. Yat Chu, and Y. Feng, *J. Cosmology Astropart. Phys.* **2016**, 057 (2016), 1509.02120.
- [27] D. Foreman-Mackey, D. W. Hogg, D. Lang, and J. Goodman, *PASP* **125**, 306 (2013), 1202.3665.
- [28] T. Nishimichi, G. D'Amico, M. M. Ivanov, L. Senatore, M. Simonović, M. Takada, M. Zaldarriaga, and P. Zhang, *Phys. Rev. D* **102**, 123541 (2020), 2003.08277.
- [29] F. Beutler, H.-J. Seo, S. Saito, C.-H. Chuang, A. J. Cuesta, D. J. Eisenstein, H. Gil-Marín, J. N. Grieb, N. Hand, F.-S. Kitaura, et al., *MNRAS* **466**, 2242 (2017), 1607.03150.
- [30] Euclid Collaboration, A. Blanchard, S. Camera, C. Carbone, V. F. Cardone, S. Casas, S. Ilić, M. Kilbinger, T. Kitching, M. Kunz, et al., *arXiv e-prints arXiv:1910.09273* (2019), 1910.09273.
- [31] Note3, this term is strictly speaking a two-loop correction and is not considered by the West-Coast team in [28]. We are not exploring here any of such modelling choices, nor other descriptions (e.g. [34]) of redshift-space distortions, leaving this for future work.
- [32] G. D'Amico, L. Senatore, P. Zhang, and T. Nishimichi, *arXiv e-prints arXiv:2110.00016* (2021), 2110.00016.
- [33] M. M. Ivanov, O. H. E. Philcox, M. Simonović, M. Zaldarriaga, T. Nishimichi, and M. Takada, *Phys. Rev. D* **105**, 043531 (2022), 2110.00006.
- [34] A. G. Sánchez, R. Scocimarro, M. Crocche, J. N. Grieb, S. Salazar-Albornoz, C. Dalla Vecchia, M. Lippich, F. Beutler, J. R. Brownstein, C.-H. Chuang, et al., *MNRAS* **464**, 1640 (2017), 1607.03147.